Modeling of External Impulse via the Concept of an Effective Mass in Sawing Task

Jae Hoon Lee*, Byung Joon Park, Byung-Ju Yi, and Il-Hong Suh**

* School of Electrical Engineering and Computer Science, Hanyang University, Seoul, Korea
(Tel : +82-31-400-5218; E-mail: bj@hanyang.ac.kr)
**Graduate School of Information and Communication, Hanyang University, Seoul, Korea
(Tel : +82-2-2290-0392; E-mail: ihsuh@hanyang.ac.kr)

Abstract: Some of manufacturing tasks such as sawing task often requires continuous impulsive motion. In case of sawing task, such impulsive motions can be observed between the teeth of the saw and the object. The amount of the external impulse exerted on the object has been treated as an important control parameter.

The purpose of this work is to introduce a new concept of an effective mass in sawing task and to suggest an external impulse model in sawing task. A normalized impulse ellipsoid reflecting the velocity direction is employed to visualize the impact geometry. Experiments are performed for soft and hard workpieces to justify the external impulse model in the sawing task. It is demonstrated through simulation and experiment that the proposed external impulse model is effective to characterize the impact property.

Keywords: Impulse, Effective Mass, Sawing Task

1. INTRODUCTION

It is believed that robot manipulators will be appropriate for the light machining tasks such as sawing, pushing/pulling, scraping, grinding, pounding, and polishing. However, for the effective operation in such tasks, we have to take into account the physical characteristics of such tasks. For example, in sawing task, continuous impulsive motion is required between the teeth of the saw and the object. Another important feature of manufacturing tasks is the plastic deformation of the object. The sawn parts are deformed permanently by the sawing.

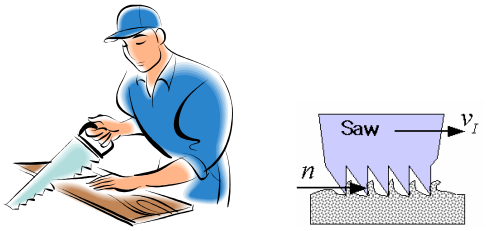

Fig. 1 Human sawing task

Fig. 1 shows the human sawing task. The external impulse acting on the object in manufacturing tasks is the function of the posture and the dynamic characteristic of the worker. That is, the capability to generate impulsive force depends on the dynamic characteristic of the manipulator (or worker). In most robot control problems dealing with impact, the robot is controlled to minimize the amount of external impulse transmitted to the robot by abrupt contact. On the contrary, the amount of external impulse should be maximized in some manufacturing tasks. However, the internal impulse experienced at the joints of the human extremity should be minimized to avoid injury or damage. For such purposes, human usually identifies how to saw and where to saw by experiences. But, the robot should be trained to perform the sawing task effectively.

Methods to evaluate the impulses occurred in general collisions have been proposed by several researchers[1-5,6,8,12,14,16]. Walker investigated the external impulse model for serial-type manipulator and also proposed an impact measure for kinematically redundant and multiple armed robotic systems[1,2,15]. Liao and Leu [3] presented the Lagrangian external impact model to derive an impact equation for an industrial manipulator. Zheng and Hemami [4] derived the internal impulse model at the joints by using Newton-Euler equations, but their model was confined to the serial-type manipulators. Wittenburg provided a general methodology in an implicit form for modeling external and internal impulses[5]. However, this model is not directly applicable to robotic systems. Kim, et al. [10] proposed a normalized impact geometry and performance measure based on velocity direction. However, their algorithm was confined to external impulse model for serial robotic system. Lee and Yi et al. [11] proposed an explicit external and internal impulse models for general classes of multi-body mechanisms.

This paper deals with a new concept of an effective mass in sawing task and suggests an external impulse model in sawing task. It is demonstrated through simulation and experiment that the proposed external impulse model is coincident to the experimental result.

2. EXTERNAL IMPULSE MODEL FOR SAWING TASK

Collision between bodies takes place in such short time interval, and the time interval is assumed to ideally go to zero. Practically deformations caused by impact propagate through the colliding bodies like waves, but it requires finite time for the waves to penetrate into the body. Therefore, the effect of the wave propagation is neglected when the impact problem is considered in macroscopic viewpoint. Thus all the bodies are assumed rigid bodies without deformations. In addition, the whole joints and the other parts of the system are assumed to have no compliance. The positions and the orientations of the colliding bodies are stationary during the time interval of impact because the velocities and the angular velocities of the bodies are finite. The variations of the velocities and the angular velocities are presumed to be discontinuous for reason that the variations take place during infinitesimal time interval. Several forces like gravity, actuating force, and action-reaction force, and so forth act on the body, but these forces are finite and cannot influence the body's motion during the time interval of impact. The only force that has an effect on the motion of the body is developed by collision, and the force

brings discontinuous change on the body's motion. This force acts for very short time but its magnitude is very large, so the integration of the force with respect to time during the infinitesimal time interval results in a finite value but zero. This force is called as *impulsive force* and the integration is named by *impulse.*

Most generally, the impact is partially elastic in the range of $0 < e < 1$. When the coefficient of restitution e is known, the relative velocity of colliding bodies can be obtained immediately after the impact. The component of the increment of relative velocity along a vector $\boldsymbol{n}$ that is normal to the contact surface is given by [5]

$$\left(\Delta \boldsymbol{\upsilon}_1 - \Delta \boldsymbol{\upsilon}_2\right)^T \boldsymbol{n} = -(1+e)\left(\boldsymbol{\upsilon}_1 - \boldsymbol{\upsilon}_2\right)^T \boldsymbol{n}, \tag{1}$$

where $\boldsymbol{\upsilon}_1$ and $\boldsymbol{\upsilon}_2$ are the absolute velocities of the colliding bodies immediately before impact, and $\Delta\boldsymbol{\upsilon}_1$ and $\Delta\boldsymbol{\upsilon}_2$ are the velocity increments immediately after impact.

When a robot system interacts with environment, the dynamic model of the robot referenced to the independent joint set is given by

$$\boldsymbol{T}_a = [\boldsymbol{I}^*_{aa}]\ddot{\boldsymbol{\phi}}_a + \dot{\boldsymbol{\phi}}_a^T [\boldsymbol{P}^*_{aaa}]\dot{\boldsymbol{\phi}}_a - [\boldsymbol{G}_a^{\upsilon_I}]^T \boldsymbol{F}_I, \tag{2}$$

where $\boldsymbol{T}_a$ denotes the inertial load vector referenced to the independent joint set. $[\boldsymbol{I}^*_{aa}]$ and $[\boldsymbol{P}^*_{aaa}]$ represent the inertia matrix and the inertia power array referenced to the independent joint set, respectively[7,13]. And $\boldsymbol{F}_I$ is the impulsive external force at the contact point and $[\boldsymbol{G}_a^{\upsilon_I}] \in \Re^{3\times N_a}$ is the 1st order KIC relating the contact point's velocity $\boldsymbol{\upsilon}_I$ with respect to the inertial frame to the independent joint's velocity.

$$\boldsymbol{\upsilon}_I = [\boldsymbol{G}_a^{\upsilon_I}]\dot{\boldsymbol{\phi}}_a. \tag{3}$$

Integration of the dynamic model given in Eq. (2) over contacting time interval gives

$$\begin{aligned}\int_{t_0}^{t_0+\Delta t} \boldsymbol{T}_a dt = &\int_{t_0}^{t_0+\Delta t} [\boldsymbol{I}^*_{aa}]\ddot{\boldsymbol{\phi}}_a dt + \int_{t_0}^{t_0+\Delta t} \dot{\boldsymbol{\phi}}_a^T [\boldsymbol{P}^*_{aaa}]\dot{\boldsymbol{\phi}}_a dt \\ &- \int_{t_0}^{t_0+\Delta t} [\boldsymbol{G}_a^{\upsilon_I}]^T \boldsymbol{F}_I dt.\end{aligned} \tag{4}$$

Since the positions and velocities are finite at all times as Δt goes to zero, the integral term involving $\dot{\boldsymbol{\phi}}_a^T [\boldsymbol{P}^*_{aaa}]\dot{\boldsymbol{\phi}}_a$ becomes zero, as does that involving actuation input $\boldsymbol{T}_a$. Thus, we obtain the following simple expression[2]

$$[\boldsymbol{I}^*_{aa}]\left(\dot{\phi}(t_0 + \Delta t) - \dot{\phi}(t_0)\right) = [\boldsymbol{G}_a^{\upsilon_I}]^T \tilde{\boldsymbol{F}}_I, \tag{5}$$

where $\tilde{\boldsymbol{F}}_I = \int_{t_0}^{t_0+\Delta t} \boldsymbol{F}_I dt$ is defined as the external impulse at the contact point. From Eq. (5), the velocity increment of the joint variables is obtained as

$$\Delta\dot{\phi}_a = [\boldsymbol{I}^*_{aa}]^{-1}[\boldsymbol{G}_a^{\upsilon_I}]^T \tilde{\boldsymbol{F}}_I, \tag{6}$$

and the velocity increment at the contact point is obtained by the following kinematic relationship.

$$\Delta\boldsymbol{\upsilon}_I = [\boldsymbol{G}_a^{\upsilon_I}]\Delta\dot{\phi}_a = [\boldsymbol{G}_a^{\upsilon_I}][\boldsymbol{I}^*_{aa}]^{-1}[\boldsymbol{G}_a^{\upsilon_I}]^T \tilde{\boldsymbol{F}}_I, \tag{7}$$

Now, let us consider a sawing task. A sawing task can be considered as a continuous collision between the teeth of the saw and the chip to be fabricated, and the impulsive force due to collision creates fracture of the chip. We assume that the fracture happens due to the shearing force formed at the bottom of the chip. That is, the lower part of a chip is fractured by the pushing of a tooth.

Based on this condition, a concept of effective mass $[\boldsymbol{M}^*_C]$ is introduced to explain the chip dynamics. Fig. 2 represents the microscopic view of a sawing task. The effective mass of the chip is defined as

$$F_c = [\boldsymbol{M}^*_C]\frac{\Delta v_c}{\Delta t_c} \tag{8}$$

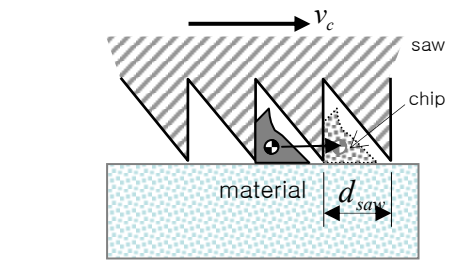

(a) Geometry of saw and chip

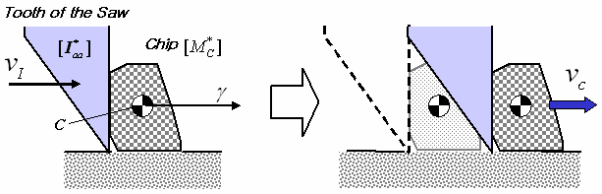

(b) Chip model

Fig. 2 Microscopic View of Sawing Task

where F_c denotes the impulsive force exerted on a chip by the tooth, v_c the velocity of the saw, Δt_c a period to saw off a piece of chip from the material, respectively. Δt_c can be computed by consideration of the geometry of saw and the sawing velocity

$$\Delta t_c = \frac{d_{saw}}{\Delta v_c}, \tag{9}$$

where d_{saw} is the distance between two adjacent teeth of the saw. , and it is given as $1mm$ in this research.

Similar to (6), the velocity increment of the joint variable of the chip is

$$\Delta\boldsymbol{\upsilon}_C = \Delta\dot{\gamma} = [\boldsymbol{M}^*_C]^{-1}(-\tilde{\boldsymbol{F}}_I), \tag{10}$$

where $[\boldsymbol{M}^*_C]$ denotes the inertia matrix of the chip to be fabricated.

Assuming that the robot impacts on a fixed solid surface, substitution of Eq. (7) and Eq. (10) into Eq. (1) gives

$$\begin{aligned}&\left\{\left([\boldsymbol{G}_a^{\upsilon_I}][\boldsymbol{I}^*_{aa}]^{-1}[\boldsymbol{G}_a^{\upsilon_I}]^T + [\boldsymbol{M}^*_C]^{-1}\right)\tilde{\boldsymbol{F}}_I\right\}^T \boldsymbol{n}. \\ &\qquad = -(1+e)\left(\boldsymbol{\upsilon}_I - \boldsymbol{\upsilon}_C\right)^T \boldsymbol{n}\end{aligned} \tag{11}$$

Then, from Eq. (11), the external impulse can be evaluated as follows:

$$\tilde{\boldsymbol{F}}_I = \left(\frac{-(1+e)(\boldsymbol{\upsilon}_I - \boldsymbol{\upsilon}_C)^T \boldsymbol{n}}{\boldsymbol{n}^T\{[\boldsymbol{G}_a^{\upsilon_I}][\boldsymbol{I}^*_{aa}]^{-1}[\boldsymbol{G}_a^{\upsilon_I}]^T + [\boldsymbol{M}^*_C]^{-1}\}\boldsymbol{n}}\right)\boldsymbol{n}, \tag{12}$$

where $[\boldsymbol{I}^*_{aa}]$ denotes the inertia matrix of the human arm grasping a saw and $[\boldsymbol{G}_a^{\upsilon_I}]$ represents the Jacobian of the contact point referenced to the joint input variables of the robot. It is noted that the external impulse is the function of robot configuration and the dynamic parameters of the sawing

task.

The value of e is 0 for purely plastic collisions (the colliding bodies have zero relative velocity to each other at the point of contact immediately after collision) and 1 for purely elastic collisions. Values of e between 0 to 1 indicate intermediate cases of the above two.

For the situation of a robot arm in contact with a solid object, such as a wall, we have the condition, $v_C = \Delta v_C = 0$. And the contact impulse force F_I is derived as

$$\tilde{F}_I = \left(\frac{-(1+e)(v_I)^T n}{n^T \left([G_a^{v_I}][I_{aa}^*]^{-1}[G_a^{v_I}]^T \right) n} \right) n . \quad (13)$$

For another situation of a robot arm in sawing task, the object to be sawn is initially stationary and the sawn chip deforms permanently. Thus, we have $v_C = 0$ and $e = 0$. The external impulse force $\tilde{F}_I$ for the sawing task is then given by

$$\tilde{F}_I = \left(\frac{-(v_I)^T n}{n^T \{ [G_a^{v_I}][I_{aa}^*]^{-1}[G_a^{v_I}]^T + [M_C^*]^{-1} \} n} \right) n , \quad (14)$$

where the first term and the second term of the denominator represents the effective dynamics contributing to the external impulse force. The first term is associated with the manipulator dynamics. In the meanwhile, the second term is associated with the material property of the chip to be sawn. Thus, the hardness of the object to be sawn changes the magnitude of the external impulsive force. Bigger impulsive force would be required to saw out the harder material as compared to soft material. The second term explains this phenomenon.

4. IMPULSE GEOMETRY AND MEASURE

Many former researchers developed various impulse geometries and impulse measures to evaluate the ability to withstand external impulse. In this chapter, we introduce various external impulse measures and impulse geometries.

Walker[1] proposed *external (dynamic) impulse ellipsoid* which represents relative magnitudes of the external impulsive forces corresponding to the unit ball of changes in joint velocities of the robot. Based on Eq. (6), the dynamic impulse ellipsoid in $\Re^m$ is described as

$$(\tilde{F}_I \in \Re^m : \tilde{F}_I^T [G_\phi^{v_I}][I_{\phi\phi}^*]^{-2}[G_\phi^{v_I}]^T \tilde{F}_I \le 1) . \quad (15)$$

From Eq. (6), the dynamic impulse ellipsoid is formed by those contact impulse forces $\tilde{F}_I$ that correspond to changes in joint velocities $\Delta\dot{\phi}$ with unit norm or less, i.e., $\left\| \Delta\dot{\phi} \right\|^2 = \Delta\dot{\phi}^T \Delta\dot{\phi} \le 1$.

However, this method does not consider the magnitude and direction of the velocity, which plays an important role in the magnitude of the external impulse. And also the magnitude of this ellipsoid does not directly represent the impact force.

Kim, et al.[10] proposed a *normalized impact geometry* for serial manipulators. Consider Fig. 3 in which let n be the unit normal vector to the environment and v_I is the pre-impulse velocity to the normal direction of the object to be fabricated. *Normalized impulse geometry* in $\Re^m$ based on $n^T v_I$ is defined by

$$\left| n^T v_I \right| \le 1 . \quad (16)$$

Then,

$$n^T ([G_\phi^{v_I}][I_{\phi\phi}^*]^{-1}[G_\phi^{v_I}]^T) n \frac{F_{imp}}{1+e} \le 1. \ (n \in \Re^m) \quad (17)$$

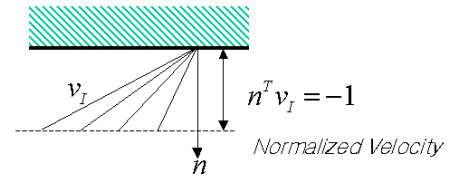

Fig. 3 Normalized task velocity

This means the range of directional impact force for given n-directional task velocity like Eq. (16). The magnitude and direction of task velocity, which play an important role in the magnitude of impulsive force, are considered in this geometry.

The normalized impact geometry can be extended to parallel manipulators. It is defined by

$$n^T ([G_a^{v_I}][I_{aa}^*]^{-1}[G_a^{v_I}]^T) n \frac{F_{imp}}{1+e} \le 1, \ (n \in \Re^m) \quad (18)$$

where, $[I_{aa}^*]$ represent the inertia matrix referenced to the independent joint set, and $[G_a^{v_I}] \in \Re^{3 \times N_a}$ is the 1st order KIC relating the contact point's velocity v_I to the independent joint's velocity, respectively.

The normalized impact geometry is obtained from Eq. (18) by calculating the maximum value of F_{imp} for each direction of n. The resulting ellipsoid is a form of belted ellipsoid.

From Eq. (12), we define the external impulse measure. In case of the sawing task, the velocity vector of the saw has the same direction as n. That is, $v_I = |v_I| n$ (refer to Fig. 1). Also note that e becomes zero in the manufacturing tasks yielding plastic deformation of the part to be fabricated. Thus, the external impulse measure for the sawing task is defined as

$$F_{imp} = \frac{-|v_I|}{n^T \{ [G_a^{v_I}][I_{aa}^*]^{-1}[G_a^{v_I}]^T + [M_C^*]^{-1} \} n} , \quad (19)$$

where, F_{imp} is the magnitude of normalized external impulse.

5. SIMULATION AND EXPERIMENTS

5.1 Simulation

Human sawing task is modeled with the parameters of male adults [9]. The numerical values of the kinematic and dynamic parameters used in simulation are presented in Table 1. Fig. 4 represents the models of human sawing tasks using single arm. Human sawing task using an arm is modeled as a 3 link planar serial manipulator. θ_1, θ_2, and θ_3 represent the shoulder joint, elbow joint, and wrist joint of the human arm, respectively. And the third link represents the human hand grasping the sawing tool. The purpose of sawing task will be to maximize the external impulse exerted on the object to be sawn by the saw.

We investigate the distribution of external impulse for the given model. It is assumed that the velocity of the moving saw is 0.6 m/s to the right direction. Coefficient of restitution e is assumed zero because of the plastic deformation of the object being sawn. Test workspace is a rectangular region given by $0.35 \le x \le 0.65$ (m) and $-0.4 \le y \le 0.4$ (m), as displayed in Fig. 4. We divide the workspace into upper

workspace (y>0) and lower workspace (y<0) in simulation. The external impulse distributions of the single arm system are depicted in Fig. 5 through Fig. 6. Here, Fig. 5 is for the case of sawing a soft material, Fig.6 is for the case of sawing a relatively hard material. The height of the plots denotes the amount of the external impulse evaluated at each position. The result of the analysis is as follows ;

(a) The lower workspace has better performance in aspect of external impulse ; compare Fig. 5(a) to Fig. 5(b). Thus, the posture of the worker and the workspace of the sawing task are important factors to maximize the external impulse.

(b) The external impulse for sawing soft materials is less than that for sawing a relatively hard material ; compare Fig. 5(b) to Fig. 6.

The characteristics of the external impulse can be also observed in terms of the impulse geometry. Fig. 7 denotes the impulse geometry described by a normalized impact geometry [10]. The dashed line denotes the external impulse. It is observed that the external ellipsoid for the optimal region is larger than that of the non-optimal region; compare Fig. 7 (a) and (b).

According to the results of the above analysis, an optimal sawing region can be identified in which the amount of external impulse is maximized. The workspace along the x direction with the value of y around -0.3m is found the optimal sawing region. This result is coincident to the human experience.

Table 1. Kinematic/Dynamic Parmeters of Human Arm Model

	Length(m)	Mass(kg)	Inertia(x,y,z ; $kg \cdot m^2$)
l_1	0.33	2.10	(0.0035,0.0208,0.0208)
l_2	0.26	1.274	(0.00136,0.00786, 0.00786)
l_3	0.5	1.70	(0.00056,0.0359,0.0355)

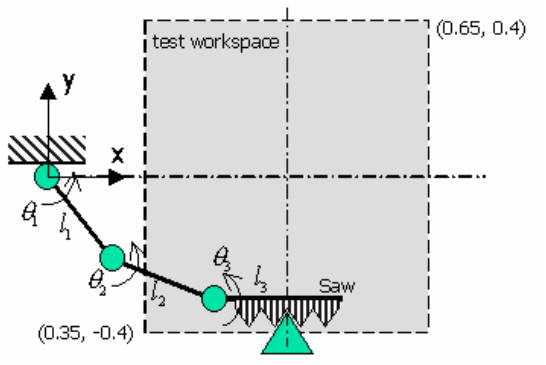

Fig. 4 Single Arm Model

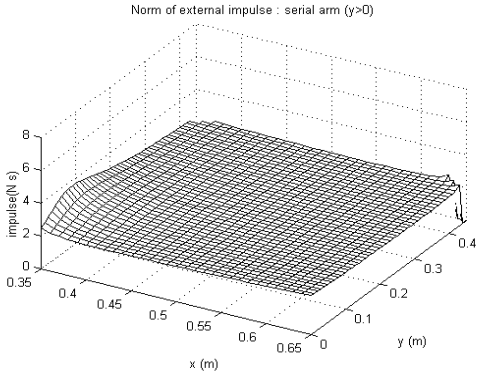

(a) Upper Region

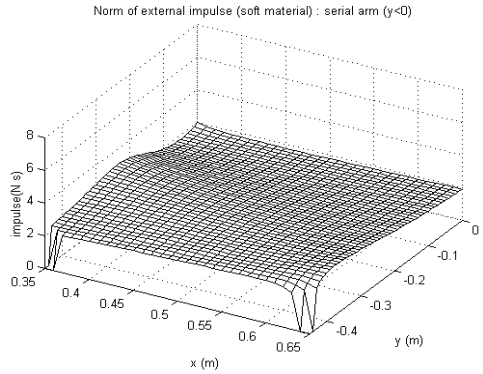

(b) Lower Region

Fig. 5 Distribution of External Impulse of Soft Material

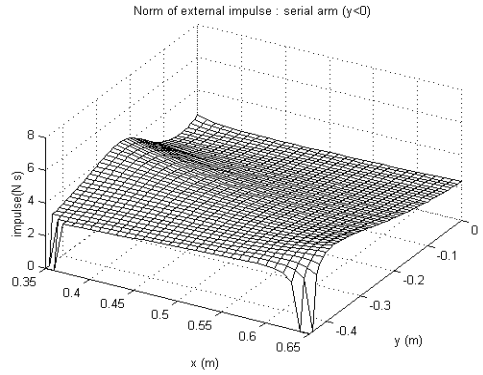

Fig. 6 Distribution of External Impulse of Hard Material (Lower Region)

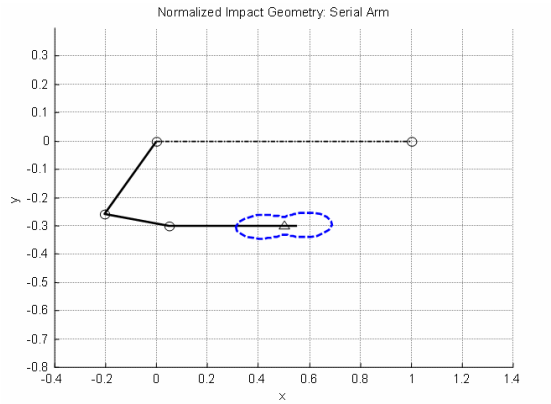

(a) Optimal Region (x, y)=(0.3, -0.3)

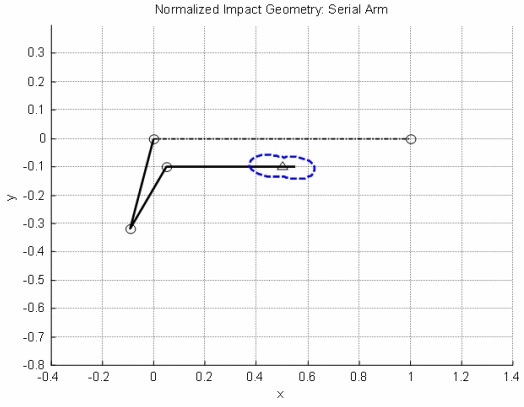

(b) Non-optimal Region (x, y)=(0.3, -0.1)
Fig. 7 Normalized External Impulse Geometry

5.2 Experiments

Fig. 8 represents a 3 DOF planar single arm system, for sawing task. Direct Drive AC motors, control hardware, and wire transmission mechanism are employed in this system. The kinematic and dynamic parameters are presented in Table 2. To measure the sawing force acting on the material, we employ a FT sensor and the material to be sawn is fixed in a gripper mounted on the force sensor.

Continuous impulse values are computed from the force data measured by the force sensor. Single arm sawing task to saw off soft and hard materials are performed. Plastic and steel slices are used as soft and hard materials, respectively. Each sawing task is executed at optimal($y = -0.25$) and non-optimal($y = -0.35$) region and performances of each task are compared. All sawing tasks are performed with velocity of $0.1m/s$ and a sawing period of 2 sec.

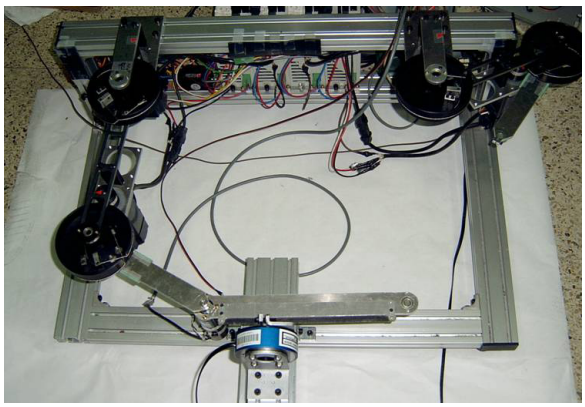

Fig. 8 Figure of Testbed for Sawing Task

Table 2 Kinematic and Dynamic Parameters of Testbed

	Length(m)	Mass(kg)	Inertia(Izz; $kg \cdot m^2$)
l_1	0.25	2.159	0.0101
l_2	0.20	0.388	0.0198
l_3	0.3	0.421	0.0359

Fig. 9 (a) represents the simulation result of the external impulse for the sawing task with soft material whose effective mass is about 0.35kg. In this graph, the solid line denotes the impulse profile of sawing in optimal region and the dashed line denotes the impulse profile of sawing in non-optimal region. Fig. 9 (b) and (c) shows experimental impulse profiles of sawing in optimal and non-optimal region, respectively. The external impulse is also calculated experimentally by measuring the force data and numerical integration of it with an interval of 10ms. It is observed from these graphs that the impulse value at the optimal region is larger than that of the non-optimal region. Thus, experimental results accord with the simulation result considerably.

Fig. 10 (a) represents the simulation and experimental results for dual arm sawing task with hard material whose effective mass is about 0.7kg. Like as Fig. 9, large external impulses are achieved at the optimal region. And external impulse profiles of sawing a hard material are larger than that of soft material.

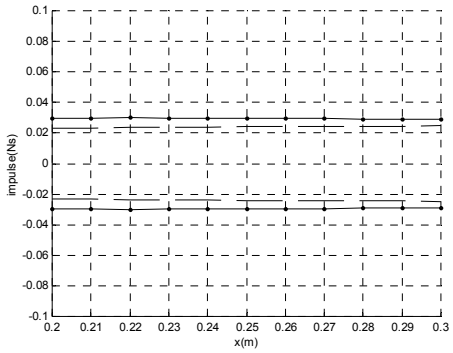

(dashed : non-optimal region, solid : optimal region)
(a) Simulation

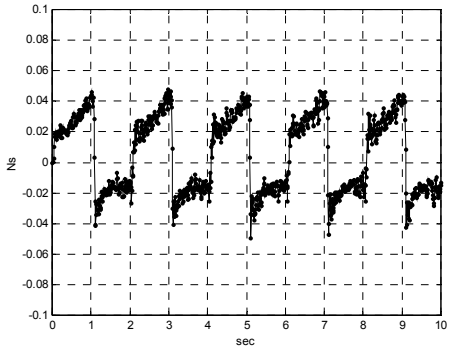

(b) Optimal Region

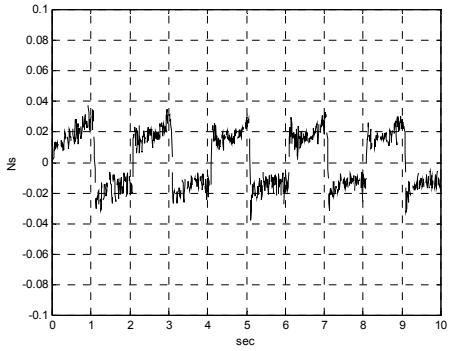

(c) Non-optimal Region
Fig. 9 External Impulse Profile for Soft Material

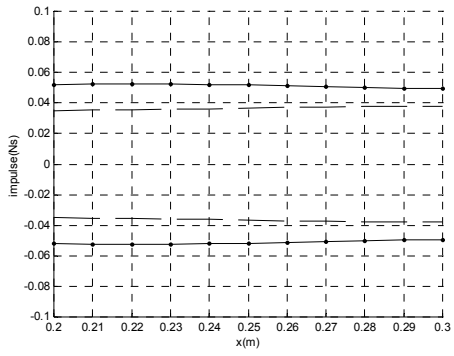

(dashed line : non-optimal region, solid line : optimal region)

(a) Simulation

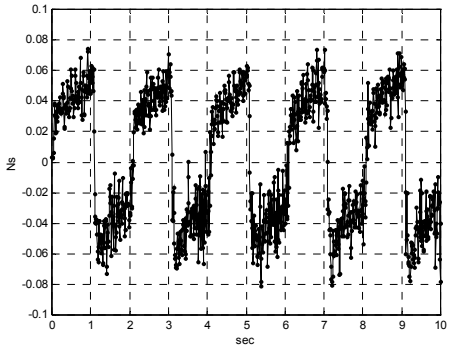

(b) Optimal Region

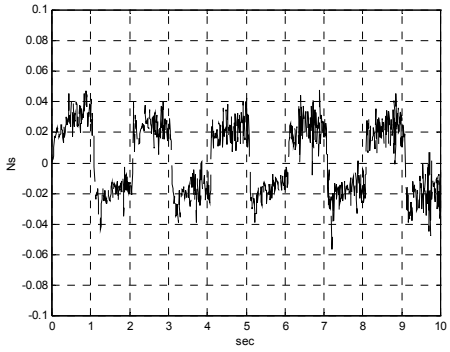

(c) Non-optimal Region

Fig. 10 External Impulse Profile of Hard Material

6. CONCLUSIONS

In the robotic manufacturing tasks such as sawing works, the amount of external impulse exerted on the object is an important parameter. In this paper, a new concept of an effective mass and an external impulse model of sawing tasks are suggested. Several simulations and experiments are performed for soft and hard workpieces to justify the external impulse model in the sawing task. It is demonstrated that the proposed external impulse model is coincident to the experimental result and human experience.

General conclusion is that the external impulse exerted on objects and joints largely depends on the geometry and dynamic characteristics of manufacturing tasks. Currently, comparative work between one arm and dual arm is ongoing.

REFERENCES

[1] I.D. Walker, "Impact configurations and measures for kinematically redundant and multiple armed robot systems", *IEEE Transactions on Robotics and Automation*, Vol. 10, No. 5, pp. 670-683, 1994.

[2] I.D. Walker, "The use of kinematic redundancy in reducing impact and contact effects in manipulation", *Proceeding of IEEE International Conference on Robotics and Automation*, pp. 434-439, 1990.

[3] H.-T. Liao and M. C. Leu, "Analysis of impact in robotic peg-in-hole assembly", *Robotica*, Vol. 16, No. 3, pp. 347-356, 1998.

[4] Y.-F. Zheng and H. Hemami, "Mathematical modeling of a robot collision with its environment", *Journal of Robotic Systems*, Vol. 2, No. 3, pp. 289-307, 1985.

[5] J. Wittenburg, *Dynamics of systems of rigid bodies*, B.G. Teubner, Stuttgart, 1977.

[6] A.R. Gravagne and I.D. Walker, "Towards Impulsive manipulation: A General Algebraic Colligion Model for Spatial Robots," *Proceeding of IEEE International conference on Roboticst and Automation*, pp. 1707-1713, 2000.

[7] H. J. Kang, B-J. Yi, W. Cho, and R. A. Freeman, "Constraint-embedding approaches for general closed-chain system dynamic in terms of a minimum set", The 1990 ASME Biennial Mechanism Conference, Chicago, IL, DE-Vol. 24, pp. 125-132, 1990.

[8] R. M. Brach, "Classical planar impact theory and the tip impact of a slender rod", *International Journal of Impact Engineering*, Vol. 13, No. 1, pp. 21-33, 1993.

[9] D.B. Chaffin, B.J. Gunnar, and Anderson, "Occupational Biomechanics", A Willey-Interscience Publication, John wiley & sons, 1984.

[10] J. Kim, W.K. Chung, and Y. Youm, "Normalized Impact Geometry and Performance Index for Redundant Manipulators," proceedings of the 2000 IEEE International Conference on Robotics and Automation, pp. 1714-1719, 2000.

[11] S.H. Lee, B.-J Yi, S.H. Kim, and Y.K. Kwak, "Modeling and Analysis of Internal Impact for General Classes of Robotic Mechanism", Proceeding of IEEE /RSJ International Conference on Robotics and Systems, pp. 1955-1962, 2000.

[12] G. Ferretti, G. Magnani, and A. Zavala Rio, "Impact modeling and control for industrial manipulators", IEEE Control System Magazine, Vol. 18, No. 4, pp. 65-71, 1998.

[13] R. A. Freeman and D. Tesar, "Dynamic modeling of serial and parallel mechanisms/robotic systems, Part I-Methodology, Part II-Applications", Proceedings on 20th ASME Biennial Mechanisms Conference, Trends and Development in Mechanisms, Machines, and Robotics, Orlando, FL, DE-Vol. 15-3, pp. 7-27, 1988.

[14] J. K. Mills and C. V. Nguyen, "Robotic manipulator collisions: Modeling and simulation", ASME Journal of Dynamic Systems, Measurement, and Control, Vol. 114, No. 4, pp. 650-659, 1992.

[15] Y. Nakamura and M. Ghodoussi, "Dynamic computation of closed-link robot mechanisms with nonredundant and redundant actuators", IEEE Transaction on Robotics and Automation, Vol. 5, No. 3, pp. 294-302, 1989.

[16] K. Youcef-Toumi and D. A. Gutz, "Impact and force control", IEEE Conference on Robotics and Automation, pp. 410-416, 1989.